Eur. Phys. J. C (2023) 83:847
https://doi.org/10.1140/epjc/s10052-023-12026-4

THE EUROPEAN PHYSICAL JOURNAL C

Regular Article - Theoretical Physics

Page curves on codim-m and charged branes

Yu Guo, Rong-Xin Miao[a]

School of Physics and Astronomy, Sun Yat-Sen University, 2 Daxue Road, Zhuhai 519082, China

Received: 30 May 2023 / Accepted: 10 September 2023 / Published online: 22 September 2023

Abstract This paper investigates Page curves on the branes with higher codimensions and charges. We study two kinds of doubly holographic modes, the AdS/dCFT and cone holography. In AdS/dCFT, the gravitations on the brane are massive, and the black hole on the codim-m brane is coupled with the non-gravitational bath on the AdS boundary. Following the standard approach, we derive the Page curve for eternal black holes. On the other hand, cone holography includes massless graviton on the brane, and the bath becomes gravitating. By adding suitable DGP gravity on the end-of-the-world brane, we recover non-trivial entanglement islands and Page curves, which strongly support that the island is consistent with massless gravity. Finally, we analyze the effects of charges and find that, as the charges increase, the Page time increases, and the parameter space for non-trivial Page curves widens.

Contents

1 Introduction

Entanglement islands are essential in addressing the black hole information paradox [1–5]. So far, most discussions in dimensions higher than two focus on doubly holographic models such as Karch–Randall (KR) braneworld [6] and AdS/BCFT [7–11]. Double holography transforms the quantum extremal surface on the branes into the classical RT surface [12] in bulk, simplifying many problems. There are two kinds of doubly holographic models. The first kinds are KR braneworld and AdS/BCFT, which contain only massive gravitations on the brane and are most studied in the literature. While the second kind includes massless gravitations on the brane [13], the typical examples are wedge holography [14,15] and cone holography [16]. Recently, [17] observes that entanglement islands disappear in the initial model of wedge holography [14], which seems to imply that entanglement islands are inconsistent with long-range massless gravity [18]. Interestingly, [19–21] find that DGP gravity [22] can resolve this problem and recover non-vanishing entanglement islands in massless gravity theories. See also [23–59] for some related works.

So far, most studies of entanglement islands and Page curves focus on codim-1 branes.[1] This paper generalizes the discussions to the brane with general codimensions and charges. The main motivation is to verify the universality of islands and to explore if higher codimensions and charges can widen the parameter space of non-vanishing islands in DGP cone holography. We investigate two kinds of models. The first model is AdS/dCFT [61,62], where the black hole on the codim-m brane is coupled with a non-gravitational bath on the AdS boundary. Similar to the usual double holography, such as KR braneworld and AdS/BCFT, the gravitations on the branes are massive. Following the standard approach, we derive the Page curves for eternal black holes [63]. Compared with the case of codim-1 brane, the new feature is that the HM surface can be defined only in a finite time for codim-m branes. Fortunately, this unusual situation does not affect Page curves since it happens after Page time. The second model is cone holography [16], where the black hole on the codim-m brane is coupled with a gravitational bath on the codim-1 brane. Cone holography is a generalization of

[a] e-mail: miaorx@mail.sysu.edu.cn (corresponding author)

[1] See some discussions on codim-2 branes [21,60].

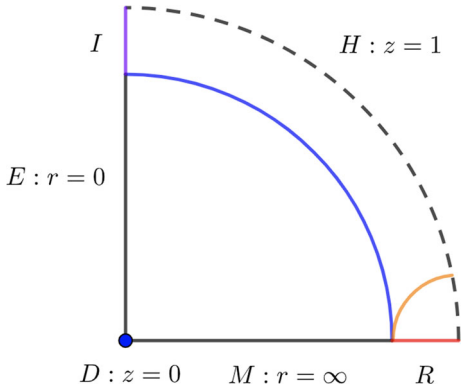

Fig. 1 AdS/dCFT and its interpretations in black hole information paradox. We focus on constant angle and time. E denotes the codim-m brane in bulk, M is AdS boundary, and $D = \partial E$ is the codim-m defect on M (D is codim-(m+1) in bulk). The purple and red lines denotes the island region I and the radiation region R, respectively. Note that the island region I and radiation region R envelop the black-hole horizon on E and M, respectively. For simplicity, we only show the regions outside the horizon. The dotted line, blue, and orange lines in the bulk indicate the horizon, the RT surface in the island phase and the HM in the no-island phase at $t = 0$, respectively

wedge holography [14,15] and includes massless gravity on the branes [16]. Following [19–21], by adding suitable DGP gravity [22] on the codim-1 brane, we recover non-trivial entanglement islands outside the horizon and time-evolving Page curves. Our results support that the entanglement island is consistent with long-range gravity theories. Finally, we discuss the effects of charges and find that charges can widen the parameter space for nontrivial Page curves.

The paper is organized as follows. In Sect. 2, we discuss Page curves for eternal black holes on codim-m branes in AdS/dCFT. In Sect. 3, we generalize the discussions to cone holography, where a massless gravitation appears on the brane and the bath becomes gravitating. By adding suitable DGP gravity, we recover entanglement islands and Page curves. In Sect. 4, we study the effects of charges in cone holography. Finally, we conclude with some open questions in Sect. 5.

2 Page curve in AdS/dCFT

To start, we first review the geometry of AdS/dCFT and its interpretation in the black hole information problem. Please see Fig. 1, where E denotes the codim-m brane in bulk, M is AdS boundary, and $D = \partial E$ is the codim-m defect on the AdS boundary M (D is codim-(m+1) in bulk). The black hole lives on the codim-m brane E, and the non-gravitational bath (non-gravitational black hole) locates at the AdS boundary. For simplicity, we focus on the black brane in bulk,

$$ds^2 = dr^2 + \sinh^2(r) d\Omega_{m-1}^2 + \cosh^2(r) \frac{\frac{dz^2}{f(z)} - f(z)dt^2 + \sum_{\hat{i}=1}^{d-1-m} dy_{\hat{i}}^2}{z^2} \tag{1}$$

where r denotes the proper distance to the codim-m brane E, $d\Omega_{m-1}^2$ is the line element of the $(m-1)$-dimensional unit sphere, $f(z) = 1 - \frac{z^{d-m}}{z_h^{d-m}}$ with horizon at $z = z_h$. For simplicity, we set $z_h = 1$ in this paper. Note that there are black holes on both the codim-m brane $E : r = 0$ and the AdS boundary $M : r = \infty$, we choose the non-gravitational black hole on the AdS boundary as the bath. We impose transparent boundary condition on the defect $D : z = 0$, so that Hawking radiation can flow from the codim-m brane E to the AdS boundary M. It is similar to the usual setup in double holography.

Let us explain the black brane (1) more. For simplicity, this paper focuses on the tensionless black brane E, where metric (1) has no conical singularity around the brane $r \to 0$ [16,60]. By performing the holographic renormalization, we can calculate the stress tensor of CFTs on the AdS boundary $r \to \infty$. Similar to the black string [30], the holographic stress tensor of CFTs is trivial up to a universal anomalous term for even d. It means the mass of the black brane (1) is also trivial, which vanishes for odd d and is independent of z_h defined in $f(z)$ for even d. It is consistent with the fact that the codim-m brane E is tensionless. Since the black brane is tensionless, there is no backreaction to the geometry in AdS/dCFT. One may ask what happens for the tensive black brane. The case of tensive codim-2 brane E is carefully studied in [60], and the Page curve is similar to the tensionless case. In comparison, there are no well-defined tensive codim-m branes with $m > 2$ for Einstein gravity [64]. For the above reasons, this paper focuses on tensionless black branes.

We aim to calculate the entanglement entropy of radiation region R (red line of Fig. 1), which is given by the area of RT surfaces in bulk. There are two kinds of RT surfaces: the one called island surface ends on the brane (blue curve of Fig. 1), while the one named Hartman–Maldacena (HM) surface (orange curve of Fig. 1) ends on the horizon at the beginning time $t = 0$, and then pass through the horizon at $t > 0$. Due to the dynamic nature of spacetime inside the horizon, the area of HM surface increases over time and exceeds the black hole entropy at late times. This is the information paradox for eternal black holes. Thanks to the island surface with a constant area, the entanglement entropy stops increasing and becomes a constant at Page time, which "resolves" the information paradox.

Let us first discuss the island surface (blue curve of Fig. 1). Assuming the embedding function $z = z(r), t = \text{constant}$, we derive the area functional from the metric (1),

$$A_{\mathrm{I}} = \int_0^{\rho_{UV}} dr \frac{\sinh^{m-1}(r)\cosh^{d-1-m}(r)}{z(r)^{d-1-m}} \sqrt{1 + \frac{\cosh^2(r) z'(r)^2}{f(z(r)) z(r)^2}}, \tag{2}$$

where I denotes the island phase, ρ_{UV} is a large cut-off for the AdS boundary, and we have set the volume of unit sphere and tangential space to be one, i.e., $V(S^{m-1}) = \int dy^{d-1-m} = 1$, for simplicity. Taking variations of (2), we derive the equation of motion (EOM)

$$\begin{aligned}
&(d-m-4)\sinh(r)\cosh^2(r)z'(r)^2z(r)^{d+m+1}\\
&+2(-d+m+2)\sinh(r)\cosh^2(r)z(r)^{2m+1}z'(r)^2\\
&-2(d-m-1)\sinh(r)z(r)^{2d+3}\\
&+4(d-m-1)\sinh(r)z(r)^{d+m+3}\\
&+2(-d+m+1)\sinh(r)z(r)^{2m+3}\\
&-\cosh(r)z(r)^{m+2}\left(z(r)^m-z(r)^d\right)\left(z'(r)(d\cosh(2r)\right.\\
&\left.-d+2m-2)+\sinh(2r)z''(r)\right)\\
&-\cosh^3(r)z(r)^{2m}z'(r)^3((d-1)\cosh(2r)\\
&-d+2m-1)=0
\end{aligned} \tag{3}$$

We impose Neumann boundary condition (NBC) on the codim-m brane E

$$z'(0) = 0, \tag{4}$$

and Dirichlet boundary condition (DBC) on the AdS boundary M

$$z(\rho_{UV}) = z_{\rm bdy}, \tag{5}$$

where $0 < z_{\rm bdy} < 1$ denotes the endpoint of island surface on the AdS boundary $M : r = \rho_{UV} \to \infty$. From EOM (3) and BCs (4, 5), we can solve numerically the island surface $z = z(r)$. Please see [60] for more calculation details, which focus on the case of codim-2 branes.

Let us go on to discuss the HM surface (orange curve of Fig. 1), which ends on the horizon at $t = 0$ and passes through the horizon at $t > 0$. According to [60], the existence of HM surface imposes a lower bound on $z_{\rm bdy}$ for codim-2 branes. We find the situation is similar for codim-m branes with $m \geq 2$. The HM surface always exits for $z_{\rm bdy} \approx 1 < 1$, and we focus on this case in this paper. To avoid coordinate singularities on horizon, we choose the infalling Eddington–Finkelstein coordinate $dv = dt - \frac{dz}{f(z)}$. Substituting the embedding functions $v = v(z)$, $r = r(z)$ into the metric (1), we obtain the area functional for HM surface

$$A_{\rm HM} = \int_{z_{\rm bdy}}^{z_{\rm max}} \frac{\sinh^{m-1}(r(z))\cosh^{d-1-m}(r(z))}{z^{d-1-m}} \times\sqrt{r'(z)^2 - \frac{\cosh^2(r(z))v'(z)\left(f(z)v'(z)+2\right)}{z^2}}dz \tag{6}$$

and the time on AdS boundary M

$$t = t(z_{\rm bdy}) = -\int_{z_{\rm bdy}}^{z_{\rm max}}\left(v'(z)+\frac{1}{f(z)}\right)dz, \tag{7}$$

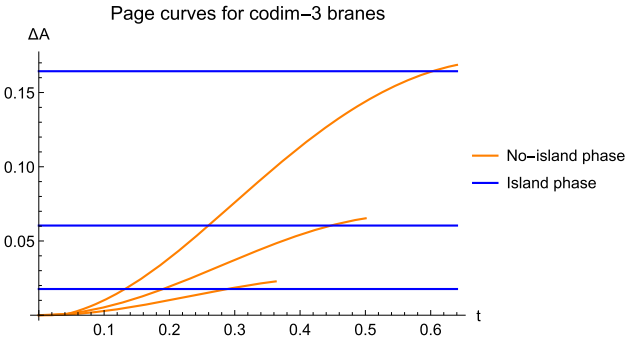

Fig. 2 Page curves on the codim-3 brane for $d = 6$ and $z_{bdy} = 0.95,\ 0.96,\ 0.97$(bottom to top). Here $\Delta A = A(t) - A(0)$, the orange curves denote the area of HM surfaces and the blue curves denote the area of island surfaces. The Page curve is given by the orange curves at $t < t_P$ and the blue curves at $t > t_P$. We observe that the Page times $t_P = 0.289, 0.448, 0.602$ increase with $z_{bdy} = 0.95,\ 0.96,\ 0.97$

where $z_{\rm max} \geq 1$ denotes the turning point of the two-side black hole. According to [65], we have $v'(z_{\rm max}) = -\infty$ and $t(z_{\rm max}) = 0$, and $z_{\rm max} = 1$ corresponds to the beginning time $t = 0$.

Since $A_{\rm HM} = \int L dz$ (6) does not depends on $v(z)$ exactly, we can define a conserved quantity

$$\begin{aligned}
E_N &= \frac{\partial L}{\partial v'(z)}\\
&= -\frac{z^{-d+m-1}\left(f(z)v'(z)+1\right)\sinh^{m-1}(r(z))\cosh^{d-m+1}(r(z))}{\sqrt{r'(z)^2-\frac{\cosh^2(r(z))v'(z)(f(z)v'(z)+2)}{z^2}}}\\
&= -\sqrt{-f\left(z_{\rm max}\right)}z_{\rm max}^{m-d}\sinh^{m-1}\left(r\left(z_{\rm max}\right)\right)\operatorname{sech}^{m-d}\left(r\left(z_{\rm max}\right)\right),
\end{aligned} \tag{8}$$

where we have used $v'(z_{\rm max}) = -\infty$. From (8), we can solve $v'(z)$ in functions of $r(z)$, $r'(z)$ and z. By using $v'(z)$ derived from (8), we simplify EOM derived from the area functional (6) as

$$\begin{aligned}
&8z^2r''\sinh(r)\left(E_N^2z^{2d}\sinh^2(r)\cosh^{2m}(r)\right.\\
&\left.+fz^{2m}\cosh^{2d}(r)\sinh^{2m}(r)\right)\\
&-4z^{2m}\cosh^{2d+1}(r)\sinh^{2m}(r)((d-1)\\
&\cosh(2r)-d+2m-1)\\
&+4zr'\sinh(r)\left(4E_N^2z^{2d}\sinh^2(r)\cosh^{2m}(r)\right.\\
&\left.+f'z^{2m+1}\cosh^{2d}(r)\sinh^{2m}(r)\right)\\
&+4zr'\sinh(r)\left(-2f(d-m-2)z^{2m}\cosh^{2d}(r)\sinh^{2m}(r)\right)\\
&-z^2\left(r'\right)^2\operatorname{sech}(r)\left(8E_N^2z^{2d}\sinh^4(r)\cosh^{2m}(r)\right.\\
&\left.+4fz^{2m}\cosh^{2d}(r)\sinh^{2m}(r)(d\cosh(2r)-d+2m-2)\right)\\
&+2z^3\left(r'\right)^3\tanh(r)\operatorname{sech}(r)\left(4E_N^2fz^{2d}\sinh^2(r)\cosh^{2m}(r)\right.\\
&\left.-2E_N^2z^{2d+1}f'\sinh^2(r)\cosh^{2m}(r)\right)
\end{aligned}$$

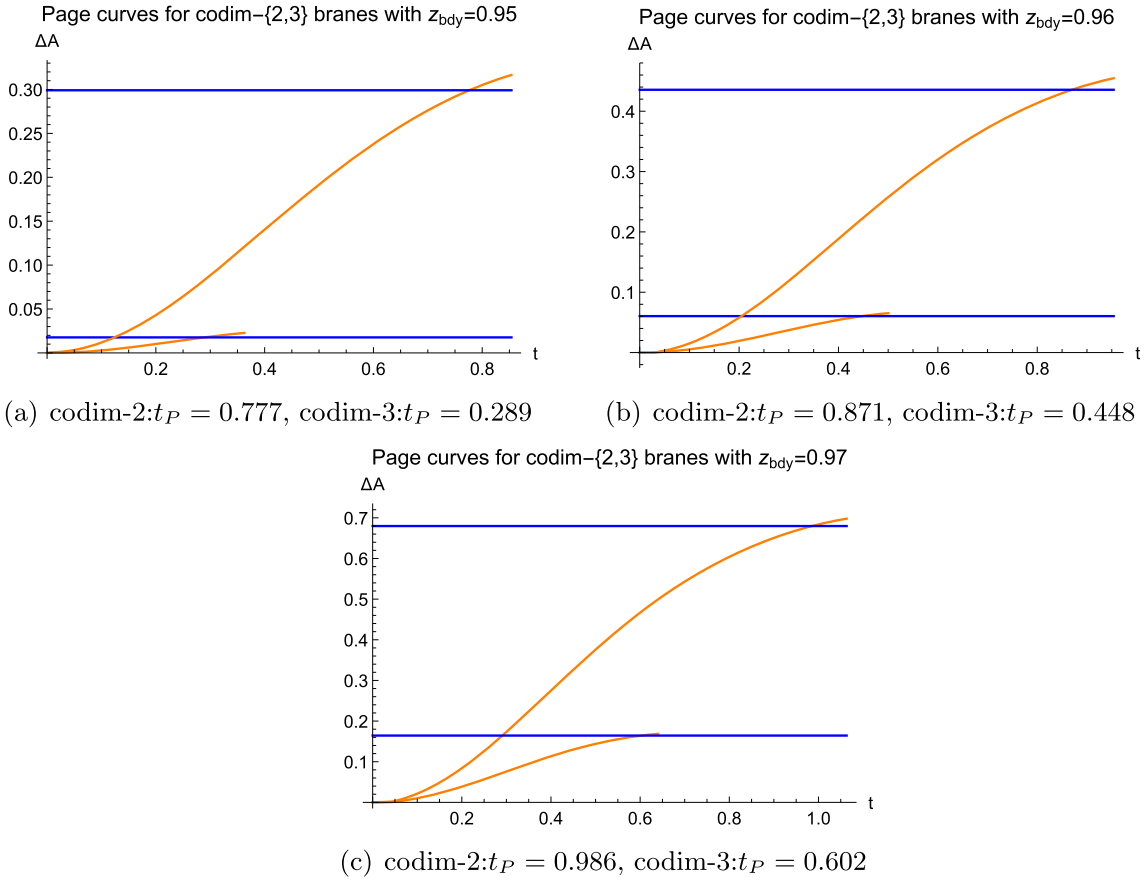

(a) codim-2:$t_P = 0.777$, codim-3:$t_P = 0.289$

(b) codim-2:$t_P = 0.871$, codim-3:$t_P = 0.448$

(c) codim-2:$t_P = 0.986$, codim-3:$t_P = 0.602$

Fig. 3 Page curves on 4-dimensional E branes with different codimensions. We take codim-2 E brane in AdS_6/CFT_5 and codim-3 E brane in AdS_7/CFT_6 as examples (top to bottom). We find that the higher the codimension, the smaller the Page time

$$+2z^3\left(r'\right)^3\tanh(r)\mathrm{sech}(r)\left(-4f^2(d-m-1)z^{2m}\times\cosh^{2d}(r)\sinh^{2m}(r)\right)=0, \tag{9}$$

where $r = r(z), r' = r'(z), f' = f'(z), f = f(z) = 1 - z^{d-m}$. Solving the above EOM perturbatively around the turning point $z = z_{\max}$, we get the BC

$$r(z_{\max}) = r_0,\quad r'(z_{\max}) = \frac{z_{\max}^{m-1}\coth(r_0)((d-1)\cosh(2r_0)-d+2m-1)}{(d-m)\left(z_{\max}^d-2z_{\max}^m\right)}. \tag{10}$$

For any given $z_{\max}$ and r_0, we can numerically solve EOM (9) with BC (10). The solution $r(z)$ does not obey the DBC $r(z_{\rm bdy}) = \rho_{UV}$ generally. So we need to adjust the input $z_{\max}$ and r_0 so that the DBC $r(z_{\rm bdy}) = \rho_{UV}$ is satisfied. This is the so-called shooting method. In this way, we numerically derive $r(z)$. Substituting $r(z)$ and $v'(z)$ derived from the conserved quantity (8) into (6) and (7), we obtain the time dependence of $A_{\rm HM}$.

Now we are ready to draw the Page curve. For simplicity, we take the codim-3 branes in $AdS_7/dCFT_6$ as examples (the spacetime on the brane E is four-dimensional). As shown in Fig. 2, the entanglement entropy of Hawking radiation first increases over time (orange curve). Then it becomes a constant (blue curve) after the Page time, recovering the expected Page curve for eternal black holes. The smaller the radiation region (the larger z_{bdy}), the larger the Page time. Besides, as shown in Fig. 3, the larger the codimensions, the shorter the Page times.

3 Page curve in cone holography

In this section, we investigate the Page curve of eternal black holes on codim-m branes in cone holography [16]. The bulk metric is still given by (1), but now the AdS boundary M at $r = \infty$ is replaced with an codim-1 brane Q at $r = \rho$, where ρ is a finite constant. Please see Fig. 4 for the geometry of cone holography. Since now the brane Q locates at finite place, there appears normalizable massless gravitation on the branes [13,20,21]. According to [17,21], since both branes are gravitating in cone holography, one should adjust both the radiation region R (red line) and the island region I (purple line) to minimize the entanglement entropy of Hawking

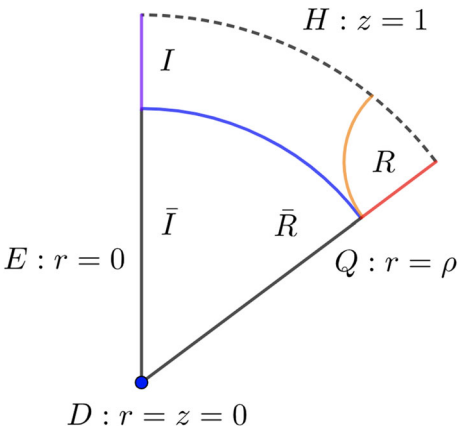

Fig. 4 Cone holography and its interpretations in black hole information paradox. We focus on constant angle and time. E denotes the codim-m brane where the black hole lives, and Q is codim-1 brane with a weak-gravity bath (weak-gravity black hole). Note that the island region I and radiation region R envelop the black-hole horizon. For simplicity, we only show the regions outside the horizon. The purple and red lines denotes the island region I and the radiation region R on E and Q, respectively. The dotted line, blue, and orange lines in the bulk indicate the horizon, the RT surface in the island phase and the HM surface in the no-island phase at $t = 0$, respectively

radiation. Furthermore, from the viewpoint of bulk, since the RT surface is minimal, it is natural to adjust its intersections ∂R and ∂I on the two branes to minimize its area. Following this approach, we recover non-trivial entanglement islands in cone holography with suitable DGP gravity. Furthermore, we work out the parameter space for Page curves, which is quite narrow.

Note that the codim-1 brane Q located at $r = \rho$ is tensive. Thus one should consider the backreaction due to the brane Q. For the end-of-the-world brane Q with only one side, the backreaction is represented by suitable boundary conditions. Following [16,21], we choose mixed boundary conditions so that (1) with brane Q at $r = \rho$ is a solution. One can also impose Neumann boundary conditions; however, the solution becomes much more complicated. There are two methods to make the brane Q obey the Neumann boundary condition. The first one considers the angle dependence for the brane location, i.e., $r = r(\theta)$ [16]. The second method adds suitable matter fields on the brane [66]. For simplicity, we focus on mixed boundary conditions in this paper, and leave the discussions of Neumann boundary condition to future work.

Let us start with the island surface (blue curve of Fig. 4). With DGP gravity on the codim-1 brane Q, the area functional of island surface becomes

$$A_{\rm I} = \int_0^{\rho} dr \frac{\sinh^{m-1}(r)\cosh^{d-1-m}(r)}{z(r)^{d-1-m}} \sqrt{1+\frac{\cosh^2(r)z'(r)^2}{f(z(r))z(r)^2}} + \frac{2\lambda \sinh^{m-1}(\rho)\cosh^{d-1-m}(\rho)}{z(\rho)^{d-1-m}}, \tag{11}$$

where λ denotes the DGP parameter, and the brane Q is at $r = \rho$. The EOM and BC on the codim-m brane E are still given by (3) and (4). Taking variations of (11), we derive the NBC on the codim-1 brane Q

$$\frac{\cosh^2(\rho)z'(\rho)}{\sqrt{\cosh^2(\rho)z'(\rho)^2 f(z(\rho)) + z(\rho)^2 f(z(\rho))^2}} - 2(d-1-m)\lambda = 0. \tag{12}$$

As mentioned above, since the brane Q is gravitating, one should adjust the endpoint $z(\rho)$ to minimize the area (11). As a result, we impose NBC (12) instead of DBC $\delta z(\rho) = 0$ in cone holography.

For $\lambda \geq 0$, we have

$$A_{\rm I} \geq \int_0^{\rho} dr \sinh^{m-1}(r)\cosh^{d-1-m}(r) + \frac{2\lambda \sinh^{m-1}(\rho)\cosh^{d-1-m}(\rho)}{z(\rho)^{d-1-m}} = A_{\rm H}, \tag{13}$$

where $A_{\rm H}$ denotes the horizon area with corrections from the DGP gravity, and we have used $f(z) \geq 0$ and $0 \leq z \leq 1$ above. The above inequality implies that the horizon is the RT surface in the island phase for $\lambda \geq 0$. As a result, the blue curve of Fig. 4 coincides with the horizon, and the island region I outside the horizon disappears.

As for $\lambda < 0$, the bulk term of (11) decreases with $z(r)$, while the boundary term of (11) increases with $z(\rho)$. These two terms compete and make it possible that there exist RT surfaces outside the horizon, i.e., $z = z(r) < 1$ for sufficiently negative λ. Below we focus on the more interesting case with $\lambda < 0$. Note that there are lower bounds for the DGP parameter λ for a well-defined theory.

Without loss of generality, we choose the parameters

$$\rho = 2.0, \quad \lambda \approx -0.122, \tag{14}$$

Solving numerically EOM (3) with BCs (4, 12), we obtain the island surface with two endpoints $z(0) \approx 0.976$ and $z(\rho) = 0.950$. Thus the radiation region is given by $z \geq z(\rho) = 0.950$.

Let us go on to discuss the HM surface in the no-island phase, whose area functional is given by

$$A_{\rm HM} = \int_{z(\rho)}^{z_{\max}} \frac{\sinh^{m-1}(r(z))\cosh^{d-1-m}(r(z))}{z^{d-1-m}} \times \sqrt{r'(z)^2 - \frac{\cosh^2(r(z))v'(z)\,(f(z)v'(z)+2)}{z^2}}\,dz + \frac{2\lambda \sinh^{m-1}(\rho)\cosh^{d-1-m}(\rho)}{z(\rho)^{d-1-m}}. \tag{15}$$

The EOM is still given by (9), but now the BC on Q becomes $r(z(\rho)) = \rho$. Similar to Sect. 2, by applying the shooting method, we can solve numerically the HM surface and then draw the Page curve as shown in Fig. 5. Following the

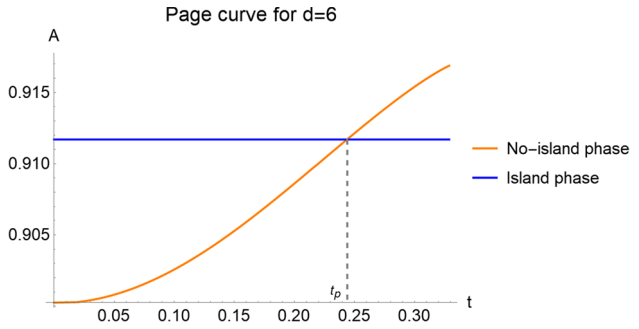

Fig. 5 Page curve on the codim-3 brane in cone holography for $d = 6$, $\rho = 2.0$, $\lambda \approx -0.122$. The orange line denotes the area of HM surface, while the blue line denotes the area of island surface. And the Page curve is given by the orange line at $t < t_P \approx 0.243$ and the blue line at $t > t_P \approx 0.243$

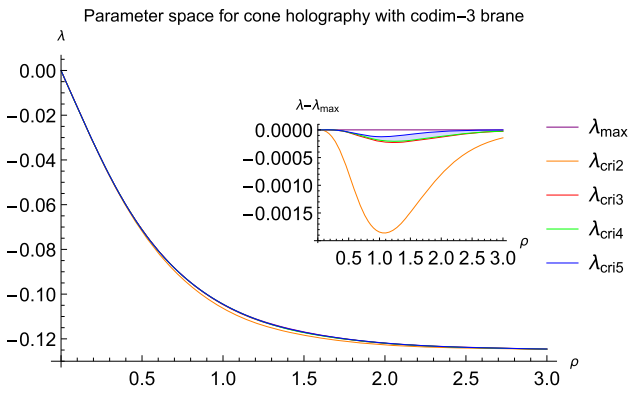

Fig. 6 Parameter space for cone holography with $m = 3$ and $d = 6$ (codim-3 branes in AdS$_7$). The purple line, orange line, red line, green line and blue line denote $\lambda_{max}, \lambda_{cri2}, \lambda_{cri3}, \lambda_{cri4}, \lambda_{cri5}$, respectively. The subplot show the difference between λ_{crii} $(i = 2, 3, 4, 5)$ and λ_{max}, where the blue belt denotes the combined constraints of parameter space. We can find the parameter space for the existence of entanglement islands and Page curves is pretty narrow. Besides, by comparing the parameter space of codim-3 brane with the one of codim-2 brane in [21], we find that the parameter space becomes narrow when the codimension increases

approach of [21], we can work out the parameter space for the DGP parameter λ. Since the calculations are similar, we do not repeat and just show the main results. First, we require the existence of islands. As discussed above, we need sufficiently negative λ in order to have non-vanishing island region outside the horizon. However, λ cannot be too negative. Otherwise, the area functional (11) of the island surface becomes negative. In this way, we derive $\lambda_{\rm cri2} < \lambda < \lambda_{\rm max}$. Second, we require that there are HM surfaces, which yields $\lambda_{\rm cri3} \leq \lambda < \lambda_{\rm max}$. Third, to have the Page curve, we require that the HM surface has a smaller area than the island surfaces at the beginning time $t = 0$, i.e., $A_{\rm N}(t = 0) < A_{\rm I}$. Then, we get $\lambda_{\rm cri4} < \lambda < \lambda_{\rm max}$. Finally, we require that $A_{\rm N}(t = 0) \geq 0$, which imposes $\lambda_{\rm cri4} < \lambda \leq \lambda_{\rm cri5}$. The strongest constraint is given by $\lambda_{\rm cri4} < \lambda \leq \lambda_{\rm cri5}$. Please see Fig. 6 for various bounds of the DGP parameter λ. We find that the parameter space becomes narrower for larger codimensions.

4 Page curve on charged branes

In this section, we discuss the Page curves and parameter space for charged branes. For simplicity, we focus on codim-2 branes with gravitational baths in cone holography. We are interested in the case of $d = 5$ so that the codim-2 brane is 4-dimensional. Solving Maxwell equations and Einstein equations, we obtain the bulk vector and metric

$$A = \left(\frac{Q}{r^3} - \frac{Q}{r_h^3}\right) d\theta, \tag{16}$$

$$ds^2 = \frac{dr^2}{f(r)} + f(r)d\theta^2 + \frac{r^2}{z^2}\left(\frac{dz^2}{1-z^3} - (1-z^3)dt^2 + dy_1^2 + dy_2^2\right), \quad r_h \leq r \leq r_0, \tag{17}$$

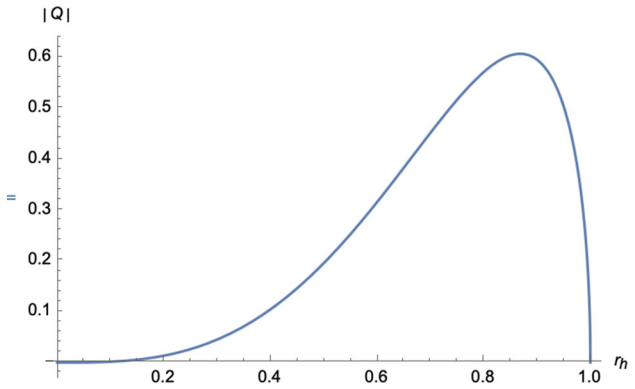

Fig. 7 The relation between $|Q|$ and r_h for the tensionless case with $n = 1$. The charge gains the maximum value $Q_{\rm max} \approx 0.607$ at $r_h \approx 0.868$. We focus on the range $0.868 \leq r_h \leq 1$, which can reduce to the charge-less case with $r_h = 1$, $Q = 0$

where Q is the "charge" parameter, $f(r) = r^2 - 1 - \frac{3}{8}\frac{Q^2}{r^6} - \frac{c_1}{r^3}$ with $c_1 = r_h^3(r_h^2 - 1 - \frac{3}{8}\frac{Q^2}{r_h^6})$ and $f(r_h) = 0$, the codim-2 brane E locates at $r = r_h$ and the codim-1 brane Q is at $r = r_0$. Note that the metric (17) takes the same form as charged hyperbolic black hole [67]. The only difference is the time $d\tau$ in Eq. (3.2) of [67] is replaced by $d\theta$ in (17) of this paper. For our case of black brane (17), there is a non-zero current density $J_\theta \sim Q$ for the dual CFTs, but the charge density is zero, i.e., $J_t = 0$. Thus, strictly speaking, the black brane (17) is uncharged. However, in this paper, we still call it "charged" black brane contrast with the charged hyperbolic black hole [67]. Similar to the case of Sect. 3, the bulk solutions (16, 17) obeys mixed boundary condition on the end-of-the-world brane Q. They can satisfy the Neumann

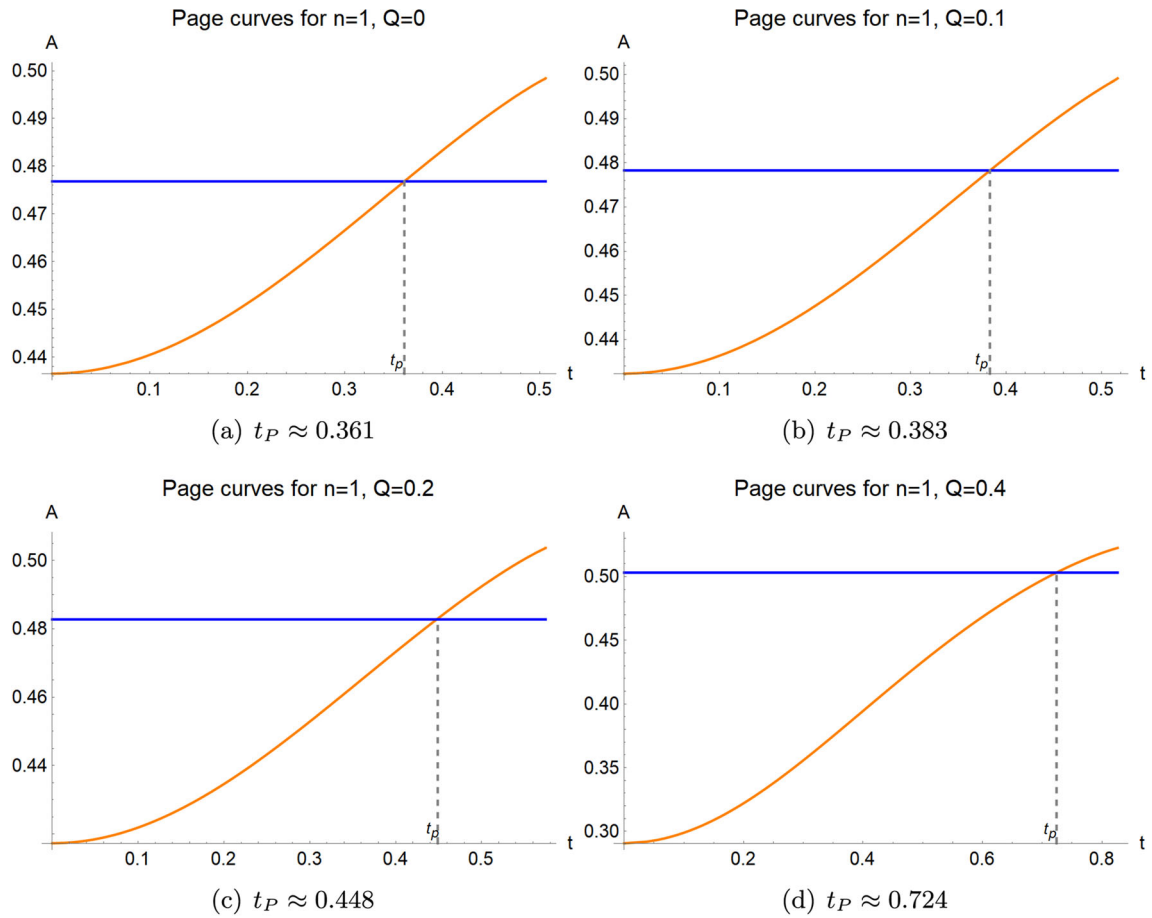

(a) $t_P \approx 0.361$ (b) $t_P \approx 0.383$

(c) $t_P \approx 0.448$ (d) $t_P \approx 0.724$

Fig. 8 Page curves for codim-2 branes with different charges. We choose $n = 1, \lambda \approx -0.161$, $r_0 = 3.0$ and $Q = 0, 0.1, 0.2, 0.4$. The blue line denotes the area of island surface and the orange line denotes the area of HM surface. The Page curve is given by the orange line when $t < t_P$ and the blue line when $t > t_P$. We find the Page time increases with the charge Q

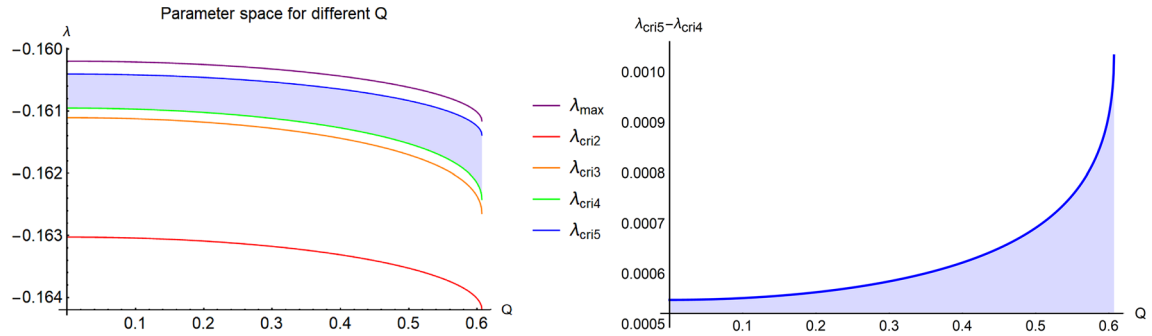

Fig. 9 Parameter space for different charges Q. The purple line, red line, orange line, green line and blue line denote λ_{max}, λ_{cri2}, λ_{cri3}, λ_{cri4}, λ_{cri5}, respectively. We set the codim-1 brane at $r_0 = 3$ and choose $n = 1$. It shows that the parameter space allowing Page curves widens as the charge increases

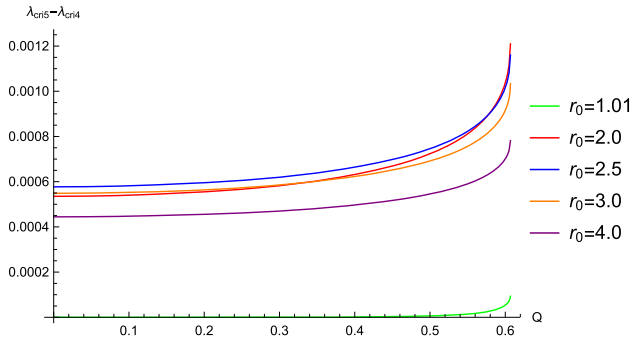

Fig. 10 The relation between the width of parameter space and charge Q. We choose $r_0 = 1.01,\ 2.0,\ 2.5,\ 3.0,\ 4.0$ and find that the width of parameter space always widens when Q increases

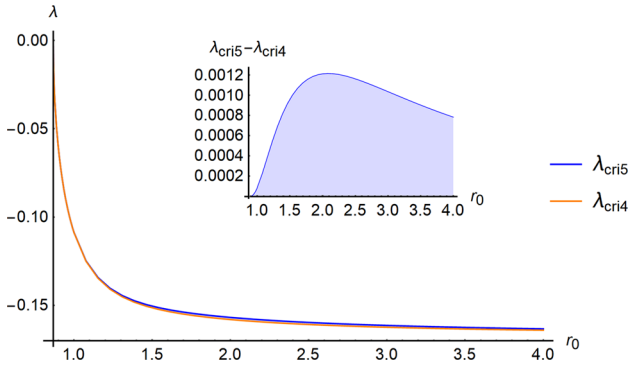

Fig. 11 Parameter space for cone holography with the maximum charge. For simplicity, we only show λ_{cri4} with orange line and λ_{cri5} with blue line, which are strongest constraints. We focus on the maximum Q, corresponding to $r_h = \frac{1}{40}\left(\sqrt{769}+7\right)$ and $Q = \frac{1}{3}\sqrt{-40r_h^8 + 16r_h^7 + 24r_h^6}$. The width of parameter space firstly increases with r_0 and then decreases with r_0

boundary condition by adding suitable matter fields on the brane [66].

To have a smooth bulk solution, we require that there is no conical singularity on the brane E, which yields

$$\frac{f'(r_h)}{4\pi} = \frac{1}{2\pi n}, \tag{18}$$

where $2\pi n$ denotes the period of θ. Note that n is related to the tension of the codim-2 brane, i.e., $8\pi G_N T_E = 2\pi(1-\frac{1}{n})$ [16]. For simplicity, we focus on the tensionless case with $n = 1$. Then (18) yields

$$|Q| = \frac{2\sqrt{2}}{3} r_h^3 \sqrt{(1-r_h)\,(3+5r_h)}, \tag{19}$$

where $0 < r_h \leq 1$. As shown in Fig. 7, the charge (19) has a maximum value $Q_{\max} \approx 0.607$ at $r_h \approx 0.868$ for $n = 1$. We focus on the range $0.868 \leq r_h \leq 1$ with larger r_h, which can reduce to the charge-less case with $r_h = 1$, $Q = 0$.

Following the approach of Sect. 3, we can derive the Page curves and parameter space for the above charged branes. We do not repeat the calculations and just show the main results below. Please see Fig. 8 for the Page curves with different charges, which shows that the Page time increases with charges. Please refer to Fig. 9 with $r_0 = 3$ and Fig. 10 with various $r_0 = 1.01,\ 2.0,\ 2.5,\ 3.0,\ 4.0$ for the parameter space of Page curves. Recall that $r = r_0$ denotes the location of the codim-1 brane. Figures 9 and 10 imply that the parameter space widens as the charge increases. Finally, we discuss the parameter space for the maximum charge in Fig. 11, which shows that the width of parameter space firstly increases with r_0 and then decreases with r_0.

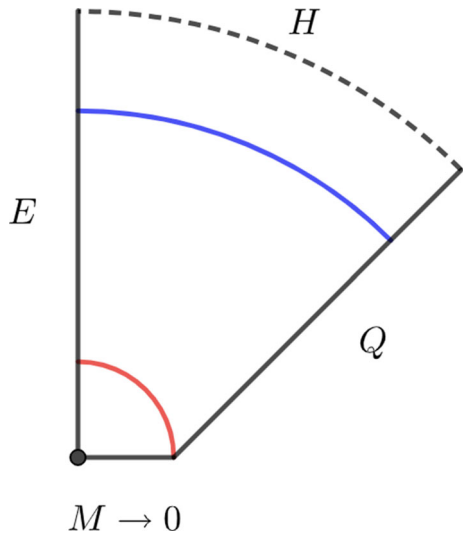

Fig. 12 Cone holography from AdS/dCFT in zero volume limit $M \to 0$. For simplicity, we focus on constant angle and time. E, Q and M denote the codim-m brane, codim-1 brane and the AdS boundary. H is the horizon, and the blue curve denotes the island surface outside the horizon. In AdS/dCFT, the causal wedge is defined by the region between the red curve and M rather than the region between the horizon and M. And the entanglement wedge is defined by the region between M and the blue curve. As a result, the causal wedge is always smaller than the entanglement wedge in AdS/dCFT. So does cone holography as a limit of AdS/dCFT

5 Conclusions and discussions

This paper investigates Page curves of eternal black holes on codim-m and charged branes in AdS/dCFT and cone holography, respectively. In AdS/dCFT, the black hole on the codim-m brane is coupled with a non-gravitating bath on the AdS boundary. Since the non-gravitating bath breaks the general covariance, the gravitons on the codim-m branes are massive. Following the standard approach, we verify that the entanglement island can recover the Page curve. Besides, we observe that the Page time decreases with codimensions but increases with z_{bdy}. On the other hand, there is a massless mode of gravitons in cone holography due to the gravitating bath on the end-of-the-world brane. By adding suitable

DGP gravity on the brane, we recover non-trivial entanglement islands and time-dependent Page curves in cone holography. Our work gives more evidence that the entanglement island is consistent with massless gravity. We also consider charged branes in cone holography and find that the Page time increases with charges. Finally, we analyze the parameter space for Page curves and see it narrows with codimensions but widens with charges. For simplicity, this paper focuses on tensionless branes and eternal black holes. Studying the case of tensive branes and evolving black holes in the future is interesting.

Note added: After this paper is finished, there appears two papers [68,69], which claim that the causal wedge is larger than the entanglement wedge whenever the island surface is outside the horizon for DGP wedge/cone holography. It is not true. A careful study of this problem in bulk shows that the causal wedge is always smaller than the entanglement wedge. Thus the DGP wedge/cone holography is well-defined. The key point is that, according to [14], wedge holography is a limit of AdS/BCFT with zero strip width. Similarly, cone holography is a limit of AdS/dCFT with a vanishing volume of dCFTs [16]. Please see Fig. 12. Since the causal wedge is always smaller than the entanglement wedge in AdS/dCFT, so does cone holography. As shown in Fig. 12, in the limit $M \to 0$, the causal wedge (region between the red curve and M) vanishes. Thus it is always smaller than the entanglement wedge (region between M and the blue curve) in cone holography. We will make more comments in future works.

Acknowledgements We thank D.q. Li for valuable discussions. R. X. Miao acknowledges the supports from National Natural Science Foundation of China (No.12275366 and No.11905297).

Data Availability Statement This manuscript has no associated data or the data will not be deposited. [Authors' comment: This is a theoretical article which does not contain experimental data and electronic supplementary material.]

Funded by SCOAP[3]. SCOAP[3] supports the goals of the International Year of Basic Sciences for Sustainable Development.

References

1. S.W. Hawking, Phys. Rev. D **14**, 2460–2473 (1976)
2. G. Penington, JHEP **09**, 002 (2020)
3. A. Almheiri, N. Engelhardt, D. Marolf, H. Maxfield, JHEP **12**, 063 (2019)
4. A. Almheiri, R. Mahajan, J. Maldacena, Y. Zhao, JHEP **03**, 149 (2020)
5. A. Almheiri, T. Hartman, J. Maldacena, E. Shaghoulian, A. Tajdini, Rev. Mod. Phys. **93**(3), 035002 (2021). arXiv:2006.06872 [hep-th]
6. A. Karch, L. Randall, JHEP **05**, 008 (2001)
7. T. Takayanagi, Phys. Rev. Lett. **107**, 101602 (2011)
8. R.X. Miao, C.S. Chu, W.Z. Guo, Phys. Rev. D **96**(4), 046005 (2017). arXiv:1701.04275 [hep-th]
9. C.S. Chu, R.X. Miao, W.Z. Guo, JHEP **04**, 089 (2017). arXiv:1701.07202 [hep-th]
10. R.X. Miao, JHEP **02**, 025 (2019). arXiv:1806.10777 [hep-th]
11. C.S. Chu, R.X. Miao, JHEP **01**, 084 (2022). arXiv:2110.03159 [hep-th]
12. S. Ryu, T. Takayanagi, Phys. Rev. Lett. **96**, 181602 (2006). arXiv:hep-th/0603001
13. P.J. Hu, R.X. Miao, JHEP **03**, 145 (2022). arXiv:2201.02014 [hep-th]
14. I. Akal, Y. Kusuki, T. Takayanagi, Z. Wei, Phys. Rev. D **102**(12), 126007 (2020). arXiv:2007.06800 [hep-th]
15. R.X. Miao, JHEP **01**, 150 (2021). arXiv:2009.06263 [hep-th]
16. R.X. Miao, Phys. Rev. D **104**(8), 086031 (2021). arXiv:2101.10031 [hep-th]
17. H. Geng, A. Karch, C. Perez-Pardavila, S. Raju, L. Randall, M. Riojas, S. Shashi, SciPost Phys. **10**(5), 103 (2021). arXiv:2012.04671 [hep-th]
18. H. Geng, A. Karch, C. Perez-Pardavila, S. Raju, L. Randall, M. Riojas, S. Shashi, JHEP **01**, 182 (2022). arXiv:2107.03390 [hep-th]
19. R.X. Miao, arXiv:2212.07645 [hep-th]
20. R.X. Miao, JHEP **03**, 214 (2023). arXiv:2301.06285 [hep-th]
21. D. Li, R.X. Miao, JHEP **06**, 056 (2023). arXiv:2303.10958 [hep-th]
22. G.R. Dvali, G. Gabadadze, M. Porrati, Phys. Lett. B **485**, 208–214 (2000)
23. A. Almheiri, R. Mahajan, J.E. Santos, SciPost Phys. **9**(1), 001 (2020). arXiv:1911.09666 [hep-th]
24. H. Geng, A. Karch, JHEP **09**, 121 (2020). arXiv:2006.02438 [hep-th]
25. H.Z. Chen, R.C. Myers, D. Neuenfeld, I.A. Reyes, J. Sandor, JHEP **10**, 166 (2020). arXiv:2006.04851 [hep-th]
26. Y. Ling, Y. Liu, Z.Y. Xian, JHEP **03**, 251 (2021). arXiv:2010.00037 [hep-th]
27. C. Krishnan, JHEP **01**, 179 (2021). arXiv:2007.06551 [hep-th]
28. K. Ghosh, C. Krishnan, JHEP **08**, 119 (2021). arXiv:2103.17253 [hep-th]
29. G. Yadav, A. Misra, Phys. Rev. D **107**(10), 106015 (2023). arXiv:2207.04048 [hep-th]
30. R. Emparan, R. Luna, R. Suzuki, M. Tomašević, B. Way, JHEP **05**, 182 (2023). arXiv:2301.02587 [hep-th]
31. E. Bahiru, A. Belin, K. Papadodimas, G. Sarosi, N. Vardian, arXiv:2301.08753 [hep-th]
32. H.Z. Chen, Z. Fisher, J. Hernandez, R.C. Myers, S.M. Ruan, JHEP **03**, 152 (2020). arXiv:1911.03402 [hep-th]
33. A. Almheiri, R. Mahajan, J. Maldacena, arXiv:1910.11077 [hep-th]
34. V. Balasubramanian, A. Kar, O. Parrikar, G. Sárosi, T. Ugajin, JHEP **01**, 177 (2021). arXiv:2003.05448 [hep-th]
35. K. Kawabata, T. Nishioka, Y. Okuyama, K. Watanabe, JHEP **05**, 062 (2021). arXiv:2102.02425 [hep-th]
36. K. Kawabata, T. Nishioka, Y. Okuyama, K. Watanabe, JHEP **10**, 227 (2021). arXiv:2105.08396 [hep-th]
37. H.Z. Chen, R.C. Myers, D. Neuenfeld, I.A. Reyes, J. Sandor, JHEP **12**, 025 (2020). arXiv:2010.00018 [hep-th]

38. H. Geng, A. Karch, C. Perez-Pardavila, S. Raju, L. Randall, M. Riojas, S. Shashi, JHEP **05**, 153 (2022). arXiv:2112.09132 [hep-th]
39. C.J. Chou, H.B. Lao, Y. Yang, Phys. Rev. D **106**(6), 066008 (2022). arXiv:2111.14551 [hep-th]
40. B. Ahn, S.E. Bak, H.S. Jeong, K.Y. Kim, Y.W. Sun, Phys. Rev. D **105**(4), 046012 (2022). arXiv:2107.07444 [hep-th]
41. M. Alishahiha, A. Faraji Astaneh, A. Naseh, JHEP **02**, 035 (2021). arXiv:2005.08715 [hep-th]
42. F. Omidi, JHEP **04**, 022 (2022). arXiv:2112.05890 [hep-th]
43. Q.L. Hu, D. Li, R.X. Miao, Y.Q. Zeng, JHEP **09**, 037 (2022). arXiv:2202.03304 [hep-th]
44. S. Azarnia, R. Fareghbal, A. Naseh, H. Zolfi, Phys. Rev. D **104**(12), 126017 (2021). arXiv:2109.04795 [hep-th]
45. T. Anous, M. Meineri, P. Pelliconi, J. Sonner, SciPost Phys. **13**(3), 075 (2022). arXiv:2202.11718 [hep-th]
46. A. Saha, S. Gangopadhyay, J.P. Saha, Eur. Phys. J. C **82**(5), 476 (2022). arXiv:2109.02996 [hep-th]
47. M.H. Yu, X.H. Ge, Phys. Rev. D **107**(6), 066020 (2023). arXiv:2208.01943 [hep-th]
48. C.S. Chu, R.X. Miao, arXiv:2209.03610 [hep-th]
49. G. Yadav, JHEP **03**, 103 (2023). arXiv:2301.06151 [hep-th]
50. Y.S. Piao, Phys. Rev. D **107**(12), 123509 (2023). arXiv:2301.07403 [hep-th]
51. A. Roy Chowdhury, A. Saha, S. Gangopadhyay, Phys. Rev. D **106**(8), 086019 (2022). arXiv:2207.13029 [hep-th]
52. S. Choudhury, S. Chowdhury, N. Gupta, A. Mishara, S.P. Selvam, S. Panda, G.D. Pasquino, C. Singha, A. Swain, Symmetry **13**(7), 1301 (2021). arXiv:2012.10234 [hep-th]
53. T.N. Hung, C.H. Nam, Eur. Phys. J. C **83**(6), 472 (2023). arXiv:2303.00348 [hep-th]
54. M. Afrasiar, J.K. Basak, A. Chandra, G. Sengupta, arXiv:2302.12810 [hep-th]
55. C. Perez-Pardavila, JHEP **05**, 038 (2023). arXiv:2302.04279 [hep-th]
56. C. Peng, J. Tian, Y. Yang, arXiv:2205.01288 [hep-th]
57. D. Basu, Q. Wen, S. Zhou, arXiv:2211.17004 [hep-th]
58. D. Basu, J. Lin, Y. Lu, Q. Wen, arXiv:2305.04259 [hep-th]
59. H.S. Jeong, K.Y. Kim, Y.W. Sun, arXiv:2305.18122 [hep-th]
60. P.J. Hu, D. Li, R.X. Miao, JHEP **11**, 008 (2022). arXiv:2208.11982 [hep-th]
61. K. Jensen, A. O'Bannon, Phys. Rev. D **88**(10), 106006 (2013). arXiv:1309.4523 [hep-th]
62. O. DeWolfe, D.Z. Freedman, H. Ooguri, Phys. Rev. D **66**, 025009 (2002). arXiv:hep-th/0111135
63. J.M. Maldacena, JHEP **04**, 021 (2003)
64. P. Bostock, R. Gregory, I. Navarro, J. Santiago, Phys. Rev. Lett. **92**, 221601 (2004). arXiv:hep-th/0311074
65. D. Carmi, S. Chapman, H. Marrochio, R.C. Myers, S. Sugishita, JHEP **11**, 188 (2017). arXiv:1709.10184 [hep-th]
66. Z.Q. Cui, R.X. Miao, in preparation
67. A. Belin, L.Y. Hung, A. Maloney, S. Matsuura, R.C. Myers, T. Sierens, JHEP **12**, 059 (2013). arXiv:1310.4180 [hep-th]
68. H. Geng, arXiv:2306.15671 [hep-th]
69. H. Geng, A. Karch, C. Perez-Pardavila, L. Randall, M. Riojas, S. Shashi, M. Youssef, arXiv:2306.15672 [hep-th]